Journal of Hazardous Materials 182 (2010) 50–54

Contents lists available at ScienceDirect

Journal of Hazardous Materials

journal homepage: www.elsevier.com/locate/jhazmat

Synthesis and photocatalytic activity of N-doped $NaTaO_3$ compounds calcined at low temperature

Da-Rui Liu, Cun-Di Wei*, Bing Xue, Xu-Guang Zhang, Yin-Shan Jiang

Key Laboratory of Automobile Materials, Ministry of Education, Department of Materials Science and Engineering, Jilin University, 5988 People's Avenue, Changchun 130025, China

ARTICLE INFO

Article history:
Received 24 February 2010
Received in revised form 26 April 2010
Accepted 29 May 2010
Available online 8 June 2010

Keywords:
$NaTaO_3$
Photocatalytic activity
Methylene blue

ABSTRACT

N-doped $NaTaO_3$ compounds ($NaTaO_{3-x}N_x$) were successfully synthesized using $NaTaO_3$ prepared at low calcination temperature as starting material and melamine ($C_3H_6N_6$) as nitrogen source. The as-prepared $NaTaO_{3-x}N_x$ samples were characterized by X-ray diffraction (XRD), X-ray photoelectron spectroscopy (XPS), scanning electron microscopy (SEM) and UV–vis diffuse reflectance spectra. The XRD results indicate that the crystallization temperature of $NaTaO_3$ is up to 700 °C and the doping of N does not lead to significant structural changes. Moreover, as observed by SEM images, the particle sizes of resultant $NaTaO_{3-x}N_x$ are in the range of 100–150 nm, which are much smaller than $NaTaO_3$ particles synthesized by traditional solid state reaction method. The photocatalytic activities of $NaTaO_{3-x}N_x$ were examined by methylene blue (MB) aqueous solution under UV light. It is found that the photocatalytic activity of $NaTaO_{3-x}N_x$ depend strongly on the doping content of N, and sample $NaTaO_{2.961}N_{0.039}$ shows the highest photocatalytic activity for the degradation of MB. Furthermore, it is also found that $NaTaO_{3-x}N_x$ catalysts display super structural stabilities during photocatalytic degradation, and could recover their photocatalytic activity after calcination at 500 °C, suggesting a promising utilization of such photocatalyst.

1. Introduction

During printing and dyeing process, nearly 15% of dyes are lost and released in the effluent water of textile industry, which usually contain reactive dyes, toxic chlorolignin, and dark coloration [1–4]. Nowadays, dye pollution has become a major source of environmental pollution in water bodies, because the conventional water treating technologies are useless in reducing the dyes content to the legal levels [5–7].

In last decades, a great deal of interest has been devoted to the photocatalytic degradation of organic water pollutants by semiconductor particles [8–10]. Among these semiconductors, the oxides of titanium (Ti), bismuth (Bi), zinc (Zn) and tin (Sn) are the preferable materials for the photocatalytic process [6,11–13]. However, the most available light sources for photocatalytic purification are UV lamps with major emission wavelength at 253.7 nm, whose energy is much higher than the band gap of semiconductors like TiO_2 (388 nm) or SnO_2 (350 nm), and thus results in the extravagance of light energies.

So far, the perovskite-type alkali tantalates, $NaTaO_3$ has received considerable attention due to its reasonable activities for water splitting into H_2 and O_2 under UV irradiation [14,15]. Traditionally, $NaTaO_3$ is produced by high temperature solid state reactions at above 1000 °C with intermittent grinding. However, such preparation method requires long time treatment and high temperature calcination, which usually results in larger grain sizes and lower photocatalytic activity [16].

Doping rare-earth or other metal oxides into the perovskite-type alkali tantalates can increase their capability of trapping and transferring electron/hole pairs, which improves their photocatalytic activities [17–22]. Recently, Torres-Martínez et al. compared the photocatalytic performances among $NaTaO_3$ samples doped with Sm and La prepared by two different methods (sol–gel and solid state reaction), was reported. The results of UV-light photocatalytic degradation reaction of methylene blue showed that the presence of La and Sm improved the photocatalytic performance of $NaTaO_3$ [23]. However, to the best of our knowledge, there are very few investigations concerning the effects of $NaTaO_3$ doped with nonmetal elements on the photocatalytic activity.

Herein, novel N-doped $NaTaO_3$ ($NaTaO_{3-x}N_x$) compounds with smaller particle sizes were synthesized from $NaTaO_3$ precursor and melamine ($C_3H_6N_6$) at 270 °C. $NaTaO_3$ precursor was prepared by an improved solid state reaction method. Such method requires low calcination temperature (only 700 °C), which is obviously lower than 1000 °C and avoidance of intermittent grinding, resulting in the improved photocatalytic activity of $NaTaO_{3-x}N_x$. The photocatalytic activity of the $NaTaO_{3-x}N_x$ catalysts was tested on the

* Corresponding author. Tel.: +86 043185094856.
E-mail addresses: yinshan_jiang@yahoo.com.cn, jiangyinshan@163.com (C.-D. Wei).

0304-3894/$ – see front matter © 2010 Elsevier B.V. All rights reserved.
doi:10.1016/j.jhazmat.2010.05.136

degradation of methylene blue (MB) aqueous solution under UV light. In order to investigate the reusable stability of catalysts, the recycling experiments were carried out.

2. Experimental

2.1. Preparation of the N-doped $NaTaO_3$ compounds

N-doped $NaTaO_3$ compounds were obtained by a mechanically induced solid state reaction. All chemicals were analytical grade reagents and used without further purification. Firstly, $NaTaO_3$ was synthesized by thermally heating a mixture of the starting materials, Ta_2O_5 and NaOH in a molar ratio of 1:2 in range of 550–1000 °C for 12 h, without intermittent grinding. Then, N-doped $NaTaO_3$ compounds were obtained by heating a mixture of the resultant $NaTaO_3$ and $C_3H_6N_6$ at 270 °C for 3 h. The molar ratio of $C_3H_6N_6/NaTaO_3$ was varied from 0 to 50%. Finally, an amount of Na (5%, sodium hydroxide) was added into the starting materials to compensate for the possible volatilization of Na_2O, and the heating rate in all the cases was 3 °C/min. The samples were cooled to room temperature and underwent characterization.

2.2. Characterization

All samples were characterized by X-ray powder diffraction (XRD). The XRD measurements were performed on a Bruke/D8-Advance with Cu Kα radiation (λ = 1.518 Å). The operation voltage and current were maintained at 40 kV and 40 mA, respectively. A scan rate of 10°/min was applied to record the patterns in the range of 2θ = 10–70°. The morphology and microstructure were characterized with scanning electronic microscope (SEM, Philips XL-30). XPS analysis was measured on a PHI 5300 ESCA instrument using an Al Ka X-ray source at a power of 250 W. The pass energy of the analyzer was set at 35.75 eV and the base pressure of the analysis chamber was $<3 \times 10^{-9}$ Torr. The binding energy scale was calibrated with respect to the C 1s peak of hydrocarbon contamination fixed at 285.0 eV. It was reported that the peak at around 400 eV corresponds to N 1s, derived from Ta–N bonds. However, because the peak area of N 1s was partly overlapped with that of Ta $4p_{3/2}$, a peak separation method was applied to calculate the peak area of N 1s. Therefore, the *x* values (nitrogen concentrations) were estimated by comparing the product of the 397.5 eV peak area multiplied by the nitrogen sensitive factor to the product of the 531 eV peak area (O 1s, Ta–O bonds) multiplied by the oxygen sensitive factor.

2.3. Photocatalytic test

The photocatalytic activities of the samples were evaluated by the decomposition of MB under UV irradiation (UVC). UV light was obtained by a 250 W high pressure mercury lamp (Philips). Aqueous suspensions (usually 100 mL) of MB (20 mg/L) and catalyst powders (100 mg) were placed in a vessel. Prior to irradiation, the suspensions were magnetically stirred in the dark for 60 min to ensure the adsorption/desorption equilibrium. At given time intervals, 3 mL of aliquots were sampled, and centrifugated to remove the particles. The filtrates were analyzed by recording the variations of the absorption band maximum (553 nm) in the UV–vis spectrum of MB using a Hitachi U-3010 spectrophotometer.

3. Results and discussion

3.1. X-ray diffraction analysis

Fig. 1 shows XRD patterns for the samples prepared at different calcination temperatures for 12 h. Clearly, the temperature

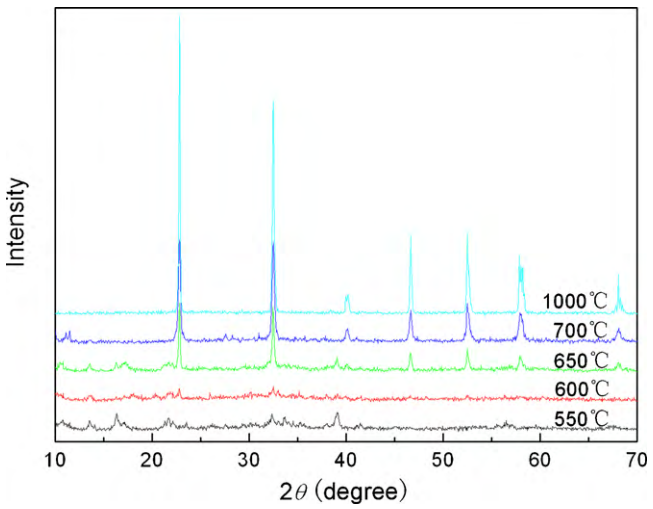

Fig. 1. XRD patterns of samples prepared at different calcination temperatures for 12 h.

exerts a great influence on the formation of $NaTaO_3$ crystalloids. All diffraction peaks of $NaTaO_3$ crystal appeared when the calcination temperature was higher than 700 °C, which could be easily indexed as a pure perovskite structure according to the standard card (JCPDS card 74-2478) [24,25]. In the range of 550–1000 °C, the intensities of the diffraction peaks became stronger with the increase of temperature, suggesting the enhanced crystallinity.

To probe the effect of the N content on the crystal structure, XRD patterns of $NaTaO_3$ with different content of N as dopant are shown in Fig. 2. As shown, the intensity of the strongest peak of $NaTaO_3$ was increased with increasing of the N content, and the replacement of O with N atom in $NaTaO_3$ did not result in significant structural changes. This could be understood that the concentration of the doped N atom (given later) might be insufficient to cause a structural rebuilding, although it has a larger ion radius of 0.171 nm than that of O atom (0.132 nm). Similar phenomena were also reported in N-doped Ta_2O_5 composite [26].

3.2. N content in the catalysts

Fig. 3 exhibits the N 1s peak around 400 eV regions in XPS spectra of N-doped $NaTaO_3$ with different N content. A new peak at

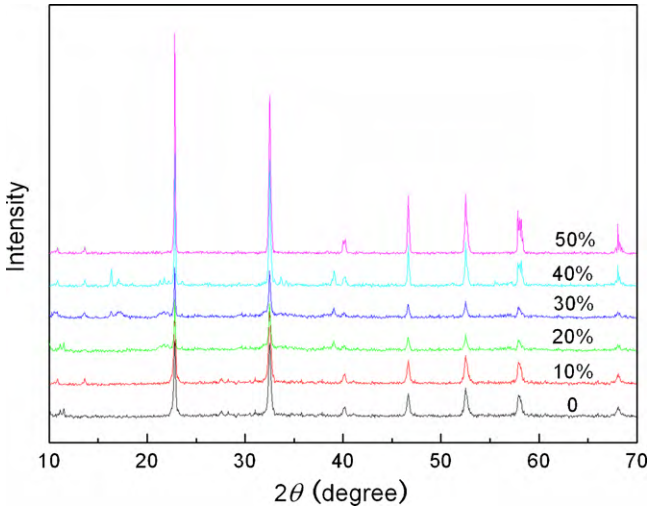

Fig. 2. XRD patterns of $NaTaO_3$ powders with different N-doped content.

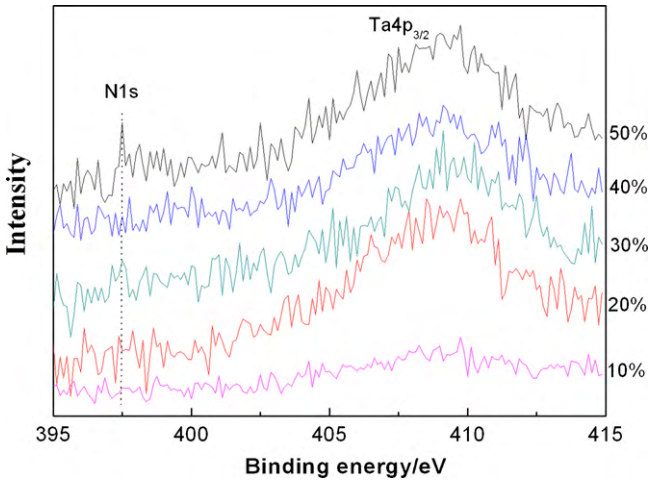

Fig. 3. N 1s peak around 400 eV regions in XPS spectra of $NaTaO_3$ powders with different N-doped content.

Table 1
The x values in $NaTaO_{3-x}N_x$ catalysts with different N-doped contents.

N addition (molar ratio)	x in the $NaTaO_{3-x}N_x$
0%	0
10%	0.012
20%	0.023
30%	0.030
40%	0.039
50%	0.054

397–398 eV was observed. This peak is generally considered as the evidence for the presence of Ta–N bonds, suggesting that the oxygen sites were substituted by nitrogen atoms [27]. Considering the results of XRD and XPS analysis, the powders were described as $NaTaO_{3-x}N_x$. The estimated x values from XPS spectra are listed in Table 1. As shown in Table 1, the resultant content of N in $NaTaO_3$ is only about 1/10 of the original chemical doping ratio due to the sublimation of melamine at 300 °C or so. The content of N in $NaTaO_3$ increases with the original chemical doping amount of N, accordingly.

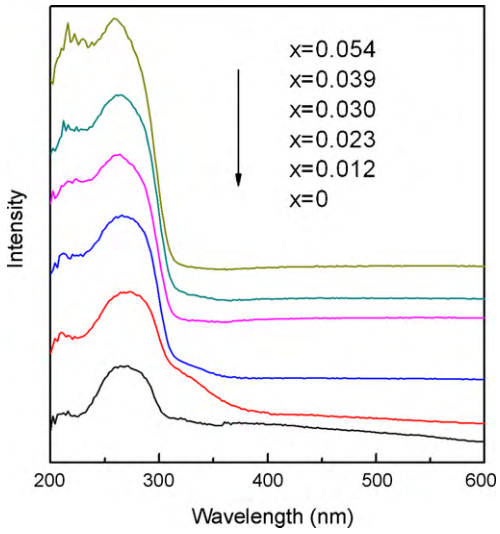

Fig. 5. UV–vis diffuse reflectance spectra of $NaTaO_{3-x}N_x$ powders.

3.3. Microstructure of the N-doped $NaTaO_3$ series photocatalysts

The morphologies of N-doped $NaTaO_3$ series photocatalysts calcined at 700 °C were determined by scanning electron microscopy (SEM). As shown in Fig. 4, all of the photocatalyst particles are very small with sizes of 100–150 nm, which is much smaller than the particle sizes synthesized by traditional solid state reaction method (usually more than 1 μm) [23].

3.4. UV–vis diffuse reflectance property

Fig. 5 shows the UV–vis diffuse reflectance spectra of the $NaTaO_{3-x}N_x$ powder samples with various N doping amounts calcined at 700 °C. It can be seen that all the samples have similar absorption edge (λ_g) in the range of 312–328 nm, which is slightly larger than that of the pure $NaTaO_3$. That means the quantum-size effects did not appear in the as-prepared $NaTaO_{3-x}N_x$ crystal, which has several hundred nanometers in size.

The band gap energy (E_g) values for the different samples were calculated from the UV–vis spectra using the equation E_g (eV) = 1240/λ_g (nm) [28]. The E_g values for the different samples

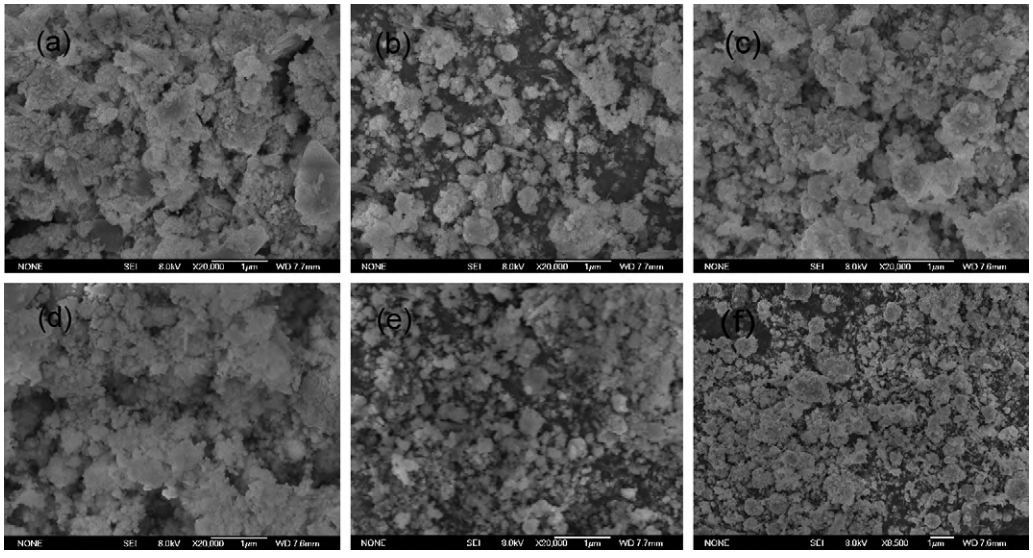

Fig. 4. SEM micrographs of the samples doped with different N contents: (a) 0%; (b) 10%; (c) 20%; (d) 30%; (e) 40% and (f) 50%.

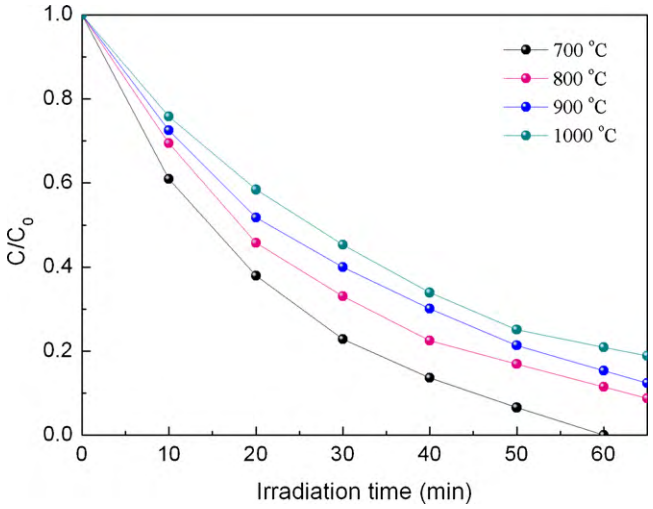

Fig. 6. The effect of calcination temperature of $NaTaO_3$ precursor on the photocatalytic activity of $NaTaO_{3-x}N_x$ under the UV-light irradiation.

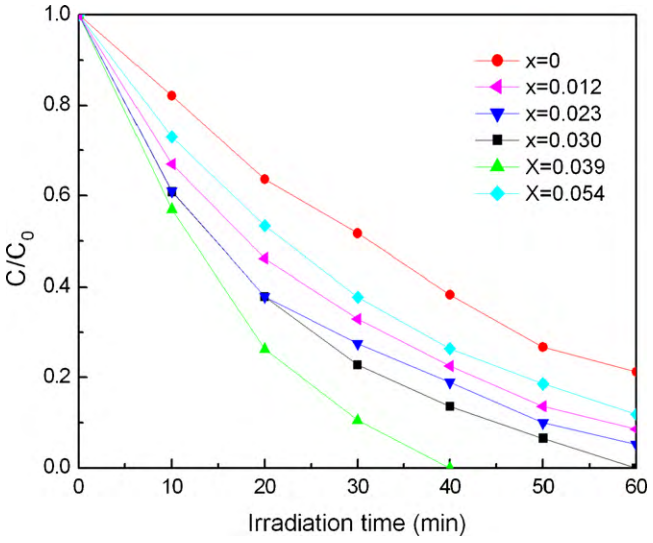

Fig. 7. The UV-light photocatalytic of as-prepared samples doped with various N contents.

are summarized in Table 2 where all the perovskite-type samples showed E_g values around 3.9 eV. Such high values indicate that these semiconductor materials are only sensitive to UV-light irradiation.

Moreover, another UV–vis absorption peak of $NaTaO_{3-x}N_x$ at 220–245 nm increases with the increasing N content, due to the combination between N and Ta. Similar phenomena are also reported for N-doped $NaTaO_3$ synthesized by hydrothermal method [29].

3.5. Photocatalytic activity

The photocatalytic activity of $NaTaO_{3-x}N_x$ was evaluated by MB degradation reaction under UV radiation. In order to investigate the effect of calcination temperature of $NaTaO_3$ precursor on the photocatalytic activity of $NaTaO_{3-x}N_x$, the experiment was performed by varying the calcination temperature of $NaTaO_3$ precursor from 700 to 1000 °C while keeping the molar ratio of $C_3H_6N_6/NaTaO_3$ was 30%. Fig. 6 shows the performance for MB decomposition depending on the calcination temperature of $NaTaO_3$ prepared. As shown in Fig. 6, with the calcination temperature of $NaTaO_3$ increasing, the photocatalytic activity of $NaTaO_{3-x}N_x$ decreased remarkably. This is due to the fact that the high temperature heat treatment may result in the grain growth, which may lead to low photocatalytic activity [16]. Therefore, the optimum calcination temperature for the production was 700 °C.

The effect of N doping on the photocatalytic activity of $NaTaO_{3-x}N_x$ was also studied. The photocatalytic degradation processes are shown in Fig. 7. It is clear that all of the N-doped $NaTaO_3$ exhibited higher photocatalytic activities than that of pure $NaTaO_3$. On the basis of the results, it is also observed that the photocatalytic efficiency was increased remarkably with the increase of N doping, when x is from 0 to 0.039. The reason is that in the case of the right nitrogen, the newly formed intra-bandgap states were found to be close enough to the conduction band edge (shallow surface states) to induce electronic coupling, which may prevent charge recombination. So the photocatalytic activity of samples was enhanced [30].

Subsequently, the photocatalytic activity was decreased drastically with the further increasing of N content, which is a similar result as for N-doped TiO_2 or Ta_2O_5 [31]. Lattice defects may act as recombination centers for photoinduced electrons and holes, leading to significant reduction [32]. The decrease of the photocatalytic activity of the sample when $x > 0.039$ may be understood in such a way, namely, that the lattice defects acting as inactivation centers were increased due to the high amount of N doping [29,33]. Therefore, among all of the samples, $NaTaO_{2.961}N_{0.039}$ showed the highest photocatalytic activity for the photodegradation of MB, and the complete degradation of MB solution was achieved in less than 40 min.

Reusable stabilities of $NaTaO_{3-x}N_x$ catalysts were also investigated. The recycling experiments on $NaTaO_{2.961}N_{0.039}$ and $NaTaO_{2.970}N_{0.030}$ were carried out under the same reaction conditions. After each reaction cycle, the catalyst was separated from the reaction mixture by centrifugation, and then reused for the next experiment with 100 mL fresh MB aqueous solution (20 mg/L). After

Table 2
The E_g values of undoped $NaTaO_3$ and N-doped $NaTaO_3$ samples.

Samples	λ_g (nm)	E_g (eV)
$NaTaO_3$	312	3.98
$NaTaO_{2.988}N_{0.012}$	328	3.78
$NaTaO_{2.977}N_{0.023}$	315	3.94
$NaTaO_{2.970}N_{0.030}$	314	3.95
$NaTaO_{2.961}N_{0.039}$	316	3.92
$NaTaO_{2.946}N_{0.054}$	316	3.92

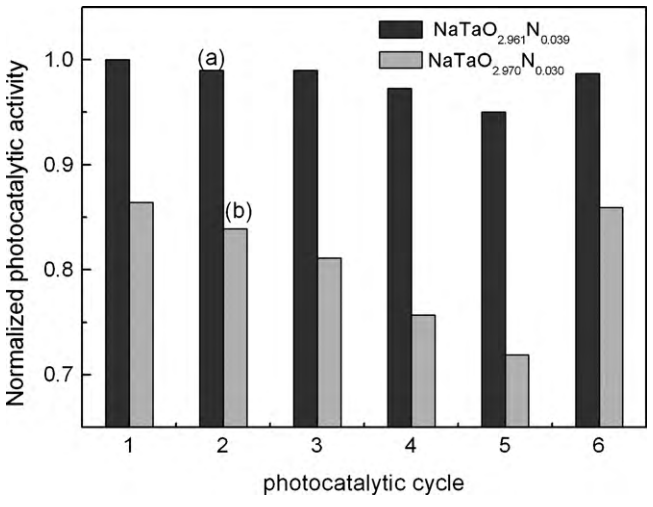

Fig. 8. The photocatalytic cycles of $NaTaO_{2.961}N_{0.039}$ (a) and $NaTaO_{2.970}N_{0.030}$ (b).

the fifth reaction cycle, the resultant sample was calcined at 500 °C to prepare for the sixth reaction cycle. The recycling photocatalytic processes of $NaTaO_{2.961}N_{0.039}$ and $NaTaO_{2.970}N_{0.030}$ are shown in Fig. 8. It can be seen that with the increase of recycling times, the photocatalytic activities of $NaTaO_{3-x}N_x$ decreased gradually. And after five cycles, the samples still remained significant photodegradation activity, suggesting that these catalysts are reasonable stable during the photocatalytic and recycling processes.

It was also found that both $NaTaO_{2.961}N_{0.039}$ and $NaTaO_{2.970}N_{0.030}$ after calcined at 500 °C display similar photocatalytic activities as the samples used for the first time, respectively. A possible explanation is that, with increasing recycling times, the organic intermediate products are prone to absorbed onto the surfaces of $NaTaO_{3-x}N_x$ during the photodegradation process of MB, and are difficult to be released even after centrifugation and washing treatment. When the catalyst is reused, these surface adsorbed organic compounds compete with MB for the active sites, therefore, decreasing the degradation rate of MB. After calcination, the surface-covered organics are decomposed at high temperature, and the $NaTaO_{3-x}N_x$ samples recover their photocatalytic activity. The $NaTaO_{3-x}N_x$ catalysts are more stable than other catalysts with perovskite structure.

4. Conclusions

$NaTaO_{3-x}N_x$ catalysts have been successfully synthesized by an improved solid state reaction method, and their photocatalytic activities were tested by the MB degradation process. The results show that doping of N increases the photocatalytic activity of $NaTaO_3$, although it displays neglectable effect on the crystal structure of $NaTaO_3$. Among all the samples, $NaTaO_{2.961}N_{0.039}$ showed the highest photodegradation rate for MB solution, and achieved the complete decolorization of MB in less than 40 min. Moreover, the structure of $NaTaO_{3-x}N_x$ catalysts is very stable during photocatalytic processes and their photocatalytic activity can be retained even after several recycling processes.

Acknowledgement

The authors gratefully thank the financially supports of National Natural Science Foundation of China (Grants Nos. 50574043 and 40772028).

References

[1] J. Nishio, M. Tokumura, H.T. Znad, Y. Kawase, Photocatalytic decolorization of azo-dye with zinc oxide powder in an external UV light irradiation slurry photoreactor, J. Hazard. Mater. 138 (2006) 106–115.
[2] N.U. Asamudo, A.S. Daba, O.U. Ezeronye, Bioremediation of textile effluent using *Phanerochaete chrysosporium*, Afr. J. Biotechnol. 4 (2005) 1548–1553.
[3] B.H. Hameed, Evaluation of papaya seeds as a novel non-conventional low-cost adsorbent for removal of methylene blue, J. Hazard. Mater. 162 (2009) 939–944.
[4] N. Nasuha, B.H. Hameed, A.T.M. Din, Rejected tea as a potential low-cost adsorbent for the removal of methylene blue, J. Hazard. Mater. 175 (2010) 126–132.
[5] D. Özer, G. Dursun, A. Özer, Methylene blue adsorption from aqueous solution by dehydrated peanut hull, J. Hazard. Mater. 144 (2007) 171–179.
[6] W.W. Zhang, J.Y. Zhang, Z.Y. Chen, T.M. Wang, Photocatalytic degradation of methylene blue by $ZnGa_2O_4$ thin films, Catal. Commun. 10 (2009) 1781–1785.
[7] A. Franco, M.C. Neves, M.M.L. Ribeiro Carrott, M.H. Mendonc, M.I. Pereiraa, O.C. Monteir, Photocatalytic decolorization of methylene blue in the presence of TiO_2/ZnS nanocomposites, J. Hazard. Mater. 161 (2009) 545–550.
[8] M.R. Hoffmann, S.T. Martin, W. Choi, D.W. Bahnemann, Environmental applications of semiconductor photocatalysis, Chem. Rev. 95 (1995) 69–96.
[9] H.H. Huang, D.H. Tseng, L.C. Juang, Heterogeneous photocatalytic degradation of monochlorobenzene in water, J. Hazard. Mater. 156 (2008) 186–193.
[10] H.R. Pouretedal, A. Norozi, M.H. Keshavarz, Abolfazl Semnan, Nanoparticles of zinc sulfide doped with manganese, nickel and copper as nanophotocatalyst in the degradation of organic dyes, J. Hazard. Mater. 162 (2009) 674–681.
[11] X.S. Hua, Y.J. Zhang, N.H. Ma, X.F. Li, H.W. Wang, A new coral structure TiO_2/Ti film electrode applied to photoelectrocatalytic degradation of reactive brilliant red, J. Hazard. Mater. 172 (2009) 256–261.
[12] L.Z. Li, B. Yan, $BiVO_4/Bi_2O_3$ submicrometer sphere composite: microstructure and photocatalytic activity under visible-light irradiation, J. Alloy Compd. 476 (2009) 624–628.
[13] L.R. Hou, C.Z. Yuan, Y. Peng, Synthesis and photocatalytic property of SnO_2/TiO_2 nanotubes composites, J. Hazard. Mater. B139 (2007) 310–315.
[14] H. Kato, K. Asakura, A. Kudo, Highly efficient water splitting into H_2 and O_2 over lanthanum-doped $NaTaO_3$ photocatalysts with high crystallinity and surface nanostructure, J. Am. Chem. Soc. 125 (2003) 3082–3089.
[15] J.W. Liua, G. Chen, Z.H. Lia, Z.G. Zhang, Hydrothermal synthesis and photocatalytic properties of $ATaO_3$ and $ANbO_3$ (A = Na and K), Int. J. Hydrogen Energy 32 (2007) 2269–2272.
[16] J.S. Xu, D.F. Xue, C.L. Yan, Chemical synthesis of $NaTaO_3$ powder at low-temperature, Mater. Lett. 59 (2005) 2920–2922.
[17] S.Y. Istomin, G. Svensson, J. Köhler, A neutron powder diffraction study of $Na_{1-x}Sr_xTaO_3$ (x = 0.2 and 0.3), Solid State Sci. 4 (2002) 191–195.
[18] R.H. Mitchell, R.P. Liferovich, A structural study of the perovskite series $Ca_{1-x}Na_xTi_{1-x}Ta_xO_3$, J. Solid State Chem. 177 (2004) 4420–4427.
[19] A. Kudo, H. Kato, Effect of lanthanide-doping into $NaTaO_3$ photocatalysts for efficient water splitting, Chem. Phys. Lett. 331 (2000) 373–377.
[20] D.G. Porob, P.A. Maggard, Flux syntheses of La-doped $NaTaO_3$ and its photocatalytic activity, J. Solid State Chem. 179 (2006) 1727–1732.
[21] S.C. Yan, Z.Q. Wang, Z.S. Li, Z.G. Zou, Photocatalytic activities for water splitting of La-doped-$NaTaO_3$ fabricated by microwave synthesis, Solid State Ion. 180 (2009) 1539–1542.
[22] Z.H. Li, Y.X. Wang, J.W. Liu, G. Chen, Y.X. Li, C. Zhou, Photocatalytic hydrogen production from aqueous methanol solutions under visible light over $Na(Bi_xTa_{1-x})O_3$ solid-solution, Int. J. Hydrogen Energy 349 (2009) 147–152.
[23] L.M. Torres-Martínez, A. Cruz-López, I. Juárez-Ramírez, Ma.E.M.la. Rosa, Methylene blue degradation by $NaTaO_3$ sol–gel doped with Sm and La, J. Hazard. Mater. 165 (2009) 774–779.
[24] S.B. Zhu, H.B. Fu, S.C. Zhang, L.W. Zhang, Y.F. Zhu, Two-step synthesis of a novel visible-light-driven $K_2Ta_2O_{6-x}N_x$ catalyst for the pollutant decomposition, J. Photochem. Photobiol. A: Chem. 193 (2008) 33–41.
[25] H. Kato, A. Kudo, Water splitting into H_2 and O_2 on alkali tantalate photocatalysts $ATaO_3$ (A = Li, Na, and K), J. Phys. Chem. B 105 (2001) 4285–4292.
[26] T. Murase, H. Irie, K. Hashimoto, Visible light sensitive photocatalysts, nitrogen-doped Ta_2O_5 powders, J. Phys. Chem. B 108 (2004) 15803–15807.
[27] J.W. Nah, W.S. Choi, S.K. Hwang, C.M. Lee, Chemical state of (Ta, Si) N reactively sputtered coating on a high-speed steel substrate, Surf. Coat. Technol. 123 (2000) 1–7.
[28] Y. He, Y.F. Zhu, N.Z. Wu, Synthesis of nanosized $NaTaO_3$ in low temperature and its photocatalytic performance, J. Solid State Chem. 177 (2004) 3868–3872.
[29] H.B. Fu, S.C. Zhang, L.W. Zhang, Y.F. Zhu, Visible-light-driven $NaTaO_{3-x}N_x$ catalyst prepared by a hydrothermal process, Mater. Res. Bull. 43 (2008) 864–872.
[30] H. Kisch, W. Macyk, Visible-light photocatalysis by modified Titania, ChemPhysChem 3 (2002) 399–400.
[31] T.J. Beck, A. Klust, M. Batzill, U. Diebold, C.D. Valentin, A. Selloni, Surface structure of TiO_2(0 1 1)-(2 × 1), Phys. Rev. Lett. 93 (2004) 1–4.
[32] S.C. Moon, H. Mametsuka, E. Suzuki, Y. Nakahara, Characterization of titanium–boron binary oxides and their photocatalytic activity for stoichiometric decomposition of water, Catal. Today 45 (1998) 79–84.
[33] R. Asahi, T. Morikawa, T. Ohwaki, K. Aoki, Y. Taga, Visible-light photocatalysis in nitrogen doped titanium oxides, Science 293 (2001) 269–271.